Deciphering relationships between the Nicobar and Bengal Submarine Fans, Indian Ocean

Kevin T. Pickering [1], Andrew Carter [2], Sergio Andò [3], Eduardo Garzanti [4], Mara Limonta [4], Giovanni Vezzoli [4], Kitty L. Milliken [5]

[1] Earth Sciences, University College London (UCL), London WC1E 6BT, UK
kt.pickering@ucl.ac.uk

[2] Dept of Earth and Planetary Sciences, Birkbeck, University of London, Malet Street, Bloomsbury, London WC1E 7HX
a.carter@ucl.ac.uk

[3] Laboratory for Provenance Studies, Department of Earth and Environmental Sciences, University of Milano-Bicocca, 210126 Milano, Italy
sergio.ando@unimib.it
eduardo.garzanti@unimib.it
mara.limonta@unimib.it
giovanni.vezzoli@unimib.it

[4] Bureau of Economic Geology, Jackson School of Geosciences, The University of Texas at Austin, 2305 Speedway Stop C1160 Austin, TX 78712-1692, USA
kittym@utexas.edu

Keywords: Nicobar Fan, Bengal Fan, sediment provenance, IODP Expedition 362, Indian Ocean, Sunda Subduction Zone

Abstract

The Nicobar Fan and Bengal fans can be considered as the eastern and western parts, respectively, of the largest submarine-fan system in the world. This study presents the integrated results of petrographic and provenance studies from the Nicobar Fan and evaluates these in the context of controls on sedimentation. Both fans were predominantly supplied by Himalaya-derived material from the main tectono-stratigraphic sequences as well as the Gangdese arc. A lack of volcanic material in the Nicobar Fan rules out sources from the Sumatra magmatic arc. Overall, the petrographic data shows a progressive decrease in sedimentary detritus and corresponding increase of higher-grade metamorphic detritus up-section. Changes in sediment provenance and exhumation rates in the Himalaya are seen to track changes in sediment accumulation rates. High sediment accumulation rates in the Bengal Fan occurred at ~13.5–8.3 Ma, and in the Nicobar Fan from ~9.5–5 Ma. Both fans show peak accumulation rates at 9.5–8.3 Ma (but with the Nicobar Fan being about twice as high), and both record a sharp drop from ~5.5–5.2 Ma, that coincided with a change in river drainage associated with the Brahmaputra River diverting west of the uplifting Shillong Plateau. At ~5 Ma, the Nicobar Fan was supplied by an eastern drainage route that finally closed at ~2 Ma, when sediment accumulation rates in the Nicobar Fan significantly decreased. Sediment provenance record these changes in routing whereby Bengal Fan deposits include granitoid sources from the Namche Barwa massif in the eastern syntaxis that are not seen in the Nicobar Fan, likely due to a more localised eastern drainage that included material from the Indo-Burman wedge. Prior to ~3 Ma, source exhumation rates were rapid and constant and the short lag-time rules out significant intermediate storage and mixing. In terms of climate *versus* tectonic controls, tectonically driven changes in the river network have had most influence on fan sedimentation.

1. Introduction

The Bengal–Nicobar Fan, Indian Ocean (Fig. 1), has the greatest length and area of any submarine fan worldwide, and has been intensively studied to investigate the possible link between Himalayan and southeast Asian tectonics, and the Asian monsoon (Curray and Moore, 1971; France-Lanord *et al*., 2016). International Ocean Discovery Program (IODP) Expedition 362 sampled the full sedimentary succession of the Nicobar Fan west of North Sumatra (Fig. 1). This work showed that starting at ~9.5 Ma, there was a dramatic and sustained rise in sediment accumulation rates (SARs) from 250–350 m/Myr until ~2 Ma that equalled or far exceeded those on the Bengal Fan at similar latitudes (McNeill *et al*., 2017a,b). This rise in SARs and a constant Himalayan-derived provenance indicates a major restructuring of the sediment routing in the Bengal–Nicobar submarine fan that was interpreted as coinciding with the uplift of the eastern Himalaya and Shillong Plateau and encroachment of the west-propagating Indo–Burmese wedge, reducing continental accommodation space and increasing sediment supply directly to the fan (*ibid*.). These results challenged the commonly held view that discrete tectonic or climatic events that impacted on the Himalayan–Tibetan Plateau caused the changes in sediment flux seen in the Bengal submarine fan.

A provenance contribution for the sediment gravity flow sandy deposits (SGF; terminology after Pickering and Hiscott, 2016) from the only previously drilled submarine fan in the eastern Indian Ocean (DSDP Site 211; referred to as the “Investigator Fan”, from the Sunda arc in the vicinity of the Andaman–Nicobar islands) cannot be entirely ruled out. However, the indistinguishable nature of the sands from DSDP sites 211 and 218 (the latter being Bengal Fan deposits) suggests that they were derived from the same Himalayan source (Ingersoll and Suczek, 1979). Lithic populations of Bengal–Nicobar sands are dominated by metasedimentary rock types, with the abundant micas (predominantly muscovite and biotite), suggesting a provenance from uplifted crystalline basement terranes of granitic to granodioritic composition, as well as extensive low- to high-grade metasedimentary terranes (Ingersoll and Suczek, 1979). The

Investigator Fan was likely a distal fan setting and, because of subduction-accretion processes, now an isolated segment of the Nicobar Fan. The oldest recovered fan sediments are ~19 Ma mud-rich SGF deposits (Pickering *et al*., 2019).

Here, we present the integrated results of studies on sediments from the Nicobar Fan, and evaluate these in the context of siliciclastic sediment provenance both to the Bengal and Nicobar fans. Figure 2 shows the potential source areas for the sediments that are considered in this paper, and Figure 3 summarises the stratigraphic units defined from IODP Expedition 362.

In order to better understand sediment source and variations in sediment flux through time and build on the initial findings of the study by McNeill *et al*. (2017b), we conducted a more extensive analysis of IODP 362 samples from sites U1480 (Fig. 3) and U1481 that extend back to 15 Ma. In addition to detrital zircon U–Pb and heavy mineral and petrographic analyses, we also applied detrital apatite fission track analysis to examine bedrock exhumation rates as this can help pinpoint sediment source areas. Detrital zircon U–Pb and apatite fission track (AFT) analyses were performed at the London Geochronology Centre at University College London, U.K. and heavy mineral and petrography data were analysed by the team at the Laboratory for Provenance Studies, University of Milano–Bicocca, Italy. Full method details are provided in the supplementary sections.

3. RESULTS

In this section, we highlight the main trends observed in the datasets. More complete descriptions of the data are provided in the Supplementary section.

3.1. Petrography

Provenance interpretation based on composition alone is made difficult by potential influences of grain size, hydraulic sorting and modification by diagenesis (Ando *et al*., 2012).

These potential influences are considered in relation to compositional trends. The succession in the Nicobar Fan can be subdivided in four petrofacies intervals (Fig. 4 and Supplementary data), from top to bottom: Petrofacies A (age < 2.39 Ma) consists of upper fine-grained feldspatho-quartzose sand rich in plagioclase and heavy minerals; Petrofacies B (age between 8.2–2.39 Ma) consists of fine-grained feldspatho-quartzose to quartz-rich feldspatho- quartzose sand; Petrofacies C (age 8.2 Ma) consists of fine-grained litho-feldspatho-quartzose to quartz-rich feldspatho-quartzose sand with more sedimentary and low-rank metasedimentary lithic grains; Petrofacies D (age > 8.2 Ma) is finer-grained and rich in feldspatho-litho-quartzose sands, and low-rank metasedimentary rock fragments.

Analysed samples are all fine-grained sands showing a coarsening-upward trend. Composition ranges from feldspatho-litho-quartzose to quartz-rich feldspatho-quartzose (Fig. 4). Metamorphic rock fragments include quartz-mica, slate, quartz-sericite, phyllite, schist, and rare garnet-bearing or sillimanite-bearing schist and gneiss. Subordinate fragments include granitoids and sedimentary rocks (i.e., shale, sparite, dolomite, siltstone, chert, micrite). Volcanic, metavolcanic, metabasite, and ultramafic lithics are rare. Among accessory grains, biotite and subordinate muscovite are invariably common, representing together 11±5 % of total framework grains. Heavy-mineral concentration estimated by point-counting ranges from 0.6–4%.

Average compositions are not significantly different throughout the sampled cores, but there are some noteworthy differences in volume percentages of total (HMC) and transparent (tHMC) heavy minerals. Moderately rich amphibole-epidote-garnet assemblages are present in the upper part of the IODP Site 1480 core (< 8.2 Ma), with the highest relative abundance (Amp 59–65% tHMC) seen in samples 80F9 and 80F52 (3.8–1.98 Ma). By contrast, epidote-amphibole-garnet assemblages are poor in the lower part of IODP sites 1480 and 1481 (10–8.2 Ma). Both cores record minor levels of apatite, tourmaline, sillimanite, clinopyroxene, zircon, titanite, staurolite, kyanite, rutile, and rare chloritoid apart from the lower part of IODP sites 1480 and 1481where tourmaline and apatite are common. Average indices for IODP samples < 8.2 Ma (sites 1480 and 1481) are tHMC (transparent Heavy Mineral Concentration) 4.0±1.4, a ZTR 6±3(Zircon-Tourmaline-Rutile index), HCI (Hornblende Colour Index) index 5±2, and Metasedimentary Minerals Index (MMI) 63±16. Broadly similar average values were measured in the older samples (10–8.2 Ma) from sites 1480 and 1481; tHMC, 1.9±0.9, the ZTR 11±5, the HCI 8±3, and the MMI index 37±19. Within samples the down-section decrease in MMI index and increase in the ZTR index (r =0.74 and 0.66) is a typical mineralogical feature of Himalayan-derived foreland-basin sediments (e.g., Szulc *et al*., 2006; Najman *et al*., 2012).

Both hydraulic-sorting processes and diagenesis may alter provenance signals. IODP Leg 362 core depths reached ~1,350 mbsf sufficient to observe diagenetic alteration and certain features are consistent with this including a progressive decrease in tHMC index with burial depth, from 4 to 1. Amphibole decreases from ~50% tHM to ~15%, while epidote increases from ≤ 20 to 48% tHM. Sillimanite becomes rare to absent at greater burial depths. Conversely, zircon, tourmaline, apatite, and chloritoid increase. However, not all minerals show the expected trends associated with diagenesis. Garnet, kyanite, staurolite, titanite, and rutile do not show significant changes with burial depth. If diagenetic alteration were important, garnet concentrations would be expected to increase. A grain-size increase is observed throughout the section and a good positive correlation is observed between grain size and heavy-mineral concentration (r = 0.79, significance level 0.1%). Garnet correlates positively with grain size both in the upper part of IODP Site 1480 core (r = 0.72, significance level. 5%) and in the lower part of both IODP sites 1480 and 1481 (r= 0.81, significance level. 2%). Conversely, epidote reaches a maximum in the finest-grained sample 81A22 (~9.5–8.5 Ma,), which is the sample with lowest heavy-mineral concentration. We interpret that the epidote/garnet ratio was controlled by grain size and hydraulic-sorting processes rather than diagenesis.

Whilst the epidote/garnet ratio has been considered as a useful parameter to distinguish between Ganges and Brahmaputra river sediments (Heroy *et al*., 2003; Garzanti *et al*., 2010), it is not possible to definitely identify changes in contributions from either the Ganges or

Brahmaputra because of these grain-size effects. After integrating petrographic and heavy-mineral evidence, the most reasonable conclusion is that vertical compositional trends show the effect of both provenance change and diagenetic bias. However, the data clearly show a progressive decrease in sedimentary detritus and corresponding up-section increase of higher-grade metamorphic detritus in the last 5.5 Ma, consistent with an increasing contribution from metamorphic source rocks found in the Greater Himalayan domain.. The Sumatra magmatic arc is an unplausible candidate, because volcanic detritus remains very minor even in Petrofacies D. To gain more insight into sand provenance we examined detrital zircon U-Pb and detrital apatite fission track signatures.

3.2. Detrital zircon U–Pb analysis

In total 32 samples were analyzed covering the time interval between 15.4–0.21 Ma. Most samples contained sufficient zircon to measure > 100 grain ages, enough to detect the main detrital age components (Table S1). Figures 5 and 6 present the data in the form of Kernel density estimates (KDE plots) and multidimensional scaling maps (Vermeesch, 2013) based on calculated K–S distances between U–Pb age spectra, comparing Nicobar Fan sand samples from this study with possible source areas compiled from the literature (Campbell *et al*., 2005; Allen *et al*., 2008; Bracciali *et al*., 2016 and references therein; Gehrels *et al*., 2011; Limonta *et al*., 2017). Although potential source areas span the drainage network of the Ganges and Brahmaputra rivers, the Brahmaputra River is considered more important as the upper Yarlung-Brahmaputra River extends into the Lhasa terrane on the Tibetan Plateau that consists of Cambrian-age granites, and Paleozoic and Mesozoic clastics intruded by Jurassic through Paleogene granitoids of the Gangdese Arc as well as younger magmatism associated with partial melting of thickened lower crust (Ji *et al*., 2019). Southwards of the Indus-Yaring suture zone are the main tectono-stratigraphic sequences of Himalayan rocks represented by (from north to south) Paleozoic and Mesozoic sedimentary rocks of the Tethyan Himalaya Sequence (THS), Late Neoproterozoic to

Ordovician high-grade metamorphic and plutonic rocks of the Greater Himalaya Sequence (GHS) and Paleoproterozoic and older metasedimentary and igneous rocks of the Lesser Himalaya Sequence (LHS). Neogene leucogranites span both the THS and GHS. The southernmost unit comprises Neogene foreland-basin sediments, such as the Siwaliks (DeCelles *et al*., 1998; Najman & Garzanti, 2000)

McNeill *et al*. (2017b) proposed that the Nicobar Fan results show a provenance from Brahmaputra River sands mixed with reworked Himalaya material originally deposited in the remnant ocean and Surma Basin (Fig. 2). A detrital zircon U–Pb study of Bengal Fan sands from IODP 354 by Blum *et al*. (2018) indicated Himalayan sources that included the eastern syntaxis, but few samples could be interpreted as representing a Ganges or Brahmaputra provenance end-member: most samples could be explained by mixing between both river systems. Figure 5 compares KDE plots of detrital zircon U–Pb data from the Bengal Fan (Blum *et al*., 2018) and Nicobar Fan (this study). The two datasets share Himalayan sources, and visually the age distributions appear similar. A more robust way to compare the age distributions are multidimensional scaling maps (MDS, Vermeesch, 2013), based on calculated K–S distances between U–Pb age spectra. If the Nicobar Fan sediments were simply the result of switching and mixing of the two river feeder systems, the MDS map would not show any major differences between Nicobar and Bengal Fan samples.

The MDS map in Figure 6A compares both the Nicobar and Bengal Fan datasets, together with modern sands from the Ganges and Brahmaputra rivers. This map shows that the two fans plot separately with little overlap. Nicobar Fan samples show greater spread in the Y-axis compared to the Bengal Fan suggesting input from additional sources to those of the Bengal Fan. Blum *et al*. (2018) suggested that the Plio-Pleistocene Ganges and Brahmaputra delivered sand to the delta independently but were later mixed, by delta-plain avulsions (including on the inner shelf delta during highstands), longshore drift or submarine gravity flows. The Bengal Fan data plot support mixing although most samples show a closer affinity to the Brahamputra River especially samples ≤ 3.2 Ma. The KDE plots show fans share the same range of Himalayan source ages (Fig. 2) differing mainly in the proportions of source ages (mainly GHS, THS, LHS). A few of the youngest Bengal Fan sediments contain ages < 10 Ma, diagnostic of the syntaxis region (Booth *et al*., 2004) that are missing from Nicobar Fan samples. Whilst similar ages can be found in the Lhasa terrane, Najman *et al*. (2019) ruled this out by using zircon fission track and rutile U-Pb ages to differentiate between syntaxial- and non-syntaxial-derived grains. Proterozoic-aged zircons are common in the Miocene Bengal Fan samples and fit with a more constant contribution (albeit low) from LHS/Ganges sources compared to the Nicobar Fan.

To further explore differences between the Bengal and Nicobar Fan zircon data, Figure 6B shows an MDS map that includes zircons from Oligocene–Pleistocene samples of the Surma Basin (peripheral Indo–Burma wedge). The Surma Basin tectono-stratigraphic units (from old to young; Barail, Bhuban, Bokabil, Tipam and Dupi Tila) share a Himalayan provenance (Najman *et al*., 2008) dominated by GHS and Trans-Himalayan arc detritus with minor contributions from the LHS (especially in the Dupi Tila), ophiolite, and possibly the eastern Himalayan or Lohit–Dianxi (Burma) batholiths (Najman *et al*., 2012; Bracciali *et al*., 2016). Also included are combined samples from the Himalayan foreland basin section at Dungsam Chu, eastern Bhutan, that are considered to represent paleo-Brahmaputra deposited after the uplift of the Shillong Plateau that caused the river to re-route to the north and west (Govin *et al*. 2018). The MDS graph (Fig. 6A) shows that samples from both fans plot in common space until a group of young Bengal Fan samples (< 3.2 Ma) plotting lower down on the Y-axis along with the modern Brahmaputra. The MDS graph in (Fig. 6C) shows the same trend. The ages of the Surma Basin units plot within the fields for both fans. To understand the nature of differences on the MDS graph Figure 6D compares the normalised percent contributions of the same age groups used by Blum *et al.* (2018), thereby permitting direct comparison with the Bengal Fan samples. The percentages are remarkably similar given the data were produced using different experimental procedures, but there are some subtle differences that help explain the MDS graphs. For example, the Nicobar Fan samples show a consistently higher proportion of ages between 400–600 Ma, typical of the GHS. Figure 6B shows that the Bengal Fan samples with ages < 4 Ma contain a significantly higher percentage of young grain ages (up to 13% compared to < 3 % in the Nicobar Fan), which can explain the trend of young (< 3.2 Ma) Bengal Fan samples.

3.3 Detrital apatite fission track data

Apatite fission track (AFT) data can help discern source areas, as AFT exhumation ages are known to vary across the Himalayan arc (Thiede and Ehlers, 2013). Table 1 summarises the detrital fission apatite fission track results. The raw data and analytical details are provided in the Supplementary section. Sample burial depths (max. 1,350 mbsf) and downhole temperatures rule out post-depositional resetting confirmed by ages older or contemporaneous with deposition age, hence the data reflect provenance. The numbers of measured grain ages varied due to abundances of suitable apatite. In most cases, however, there were sufficient numbers of grains to define the principal age component quantified using the minimum age model based on a four-parameter probability distribution (Galbraith, 2005), implemented in DensityPlotter (Vermeesch, 2012). The minimum age is a more robust indicator of youngest age components where single grain spontaneous tracks have zero or low track counts. Grain counts were pooled together for samples with the same or similar deposition ages. Figure 7 is a plot of lag-time between sample depositional age and AFT age components each diagnostic of the time taken for exhumation, routing and deposition within the Nicobar Fan. The main population of apatites in all samples show a younging trend with a near to constant lag time of 1–2 Myr that records rapid exhumation in the apatite source areas. This pattern rules out significant intermediate storage prior to deposition within the Nicobar Fan. The second most abundant population of Miocene age also shows a constant younging trend. Together these data show that there was very little mixing occurring within the submarine fan. If this were the case the age that components of older samples would also be present in younger sands and there would not be any systematic trend.

Older grains with ages between 35±10 and 337±65 Ma were also present in some samples mostly represented by single grains. Also shown Table 1, the main populations of apatites found in unreset Plio–Pleistocene foreland basins that characterize bedrock exhumation (mainly GHS as apatite is uncommon in LHS rocks) at the time they were deposited (Chirouze *et al*., 2013; Coutand *et al*., 2016). In all cases these data are closely similar to the dominant minimum age population seen in fan samples of equivalent deposition age.

4. Discussion

Compositional data confirm that the Nicobar Fan was a major sink for Himalaya-derived material since the Miocene. Vertical compositional trends show the effect of both provenance change and diagenetic bias due to dissolution of less durable detrital minerals as well as grain size and hydraulic-sorting processes (see Supplementary section for further details). As a consequence more durable heavy minerals, including zircon, tourmaline, apatite, garnet and epidote tend to be relatively enriched with increasing age and burial depth. Epidote tends to increase in finer-grained samples and where heavy-mineral concentration is lower, and likewise garnet increases in coarser-grained samples and where heavy-mineral concentration is higher. Despite such influences there is a clear upward increase in higher-grade metamorphic detritus from ~ 5.5 Ma (mainly hornblende, epidote, garnet, apatite, clinopyroxene, tourmaline, sillimanite, kyanite, zircon, titanite, and rare staurolite and rutile) consistent with Himalayan sources. The origin of sedimentary to low-grade metasedimentary detritus, the importance of which decreases progressively upwards, has yet to be ascertained, and the rare volcanic detritus rules out the Sumatra magmatic arc as a major contributor. Petrographic data suggests that sandy sediments reaching the Bengal shelf, and the Bengal and Nicobar fans, most closely match in composition those of the Brahmaputra sediments (Thompson, 1974; Ingersoll and Suczek, 1979; Yokohama *et al*., 1990; Garzanti, 2019).

Comparison of Bengal and Nicobar Fan detrital zircon datasets showed they share the same range of Himalayan source ages (Fig. 2) but there are also differences. Some Bengal Fan samples included ages < 10 Ma diagnostic of the syntaxis region (Booth *et al*., 2004) that are missing from the Nicobar Fan This absence is unlikely to be a sampling artifact given that >100 grain ages were measured in most samples, which gives a 95% certainty that no fraction of a population is missed. Proterozoic-aged zircons are more common in Bengal Fan samples and fit with a more constant contribution from LHS and Ganges sources. Combined U–Pb and thermochronometry work on the Bengal Fan samples (Najman *et al*., 2019) also found a significant component of grains derived from the TransHimalaya, supplied by drainages associated with the upper reaches of the Yarlung–Brahmaputra River in addition to some contribution from erosion of the Indo–Burma ranges. Whilst this background signal was present throughout the drilled section of the Bengal Fan, notable differences in proportions of zircon ages were considered to reflect differences in the loci of sediment production possibly driven by climate change. The same could also be argued for the Nicobar Fan.

Both the Bengal and Nicobar fans show significant temporal changes in sediment accumulation rates. The changes, however, are not always synchronous, as seen in Figure 8 that compares sediment mass accumulation rates (MARs) for the two systems (after Pickering *et al*., 2019). Mass accumulation rate (MAR) is related to the equation and calculations given in Pickering *et al*. (2019), whereas sediment accumulation rate (SAR) is used in this paper as a more general term. Whilst avulsion processes on the fans might account for some of the differences, we believe that a comparison of MARs from the Bengal and Nicobar fans is reasonable, because IODP Site U1451 (Bengal Fan) and IODP Site U1480 (Nicobar Fan) were drilled at comparable distances from the main sediment source, in similar latitudes, in similar fan environments, at a distance west of the NinetyEast Ridge that compares well with IODP Site 362 east of the ridge. Also, IODP Site U1451 penetrated ~300 m deeper than any other site on the Bengal Fan, and has the most complete stratigraphic record (and with greater core recovery, i.e., 86% with 337.80 m core recovered in Hole U1451A *versus* 64% with 282.73 m core recovered in Hole U1450A, then 29% with 180.86 m core recovered in Hole U1451A *versus* 23% with 46.67 m core recovered in Hole U1450A: see table 1 in IODP 354 Preliminary Report, 2015). Significant sediment mass accumulation rates occurred earlier in the Bengal Fan (from ~13.5– 8.3 Ma), with peak MARs reached in both fans over the same time interval, from ~9.5–8.3 Ma. However, between ~5-9.5 Ma, MARs appears significantly higher in the Nicobar Fan (Fig. 8). Similarly both fans show a marked fall in MARs at ~5.5–5.2 Ma. After this, MARs in the Bengal Fan remained low but in the Nicobar Fan they increased again from ~3.8 Ma and peaked between ~2.4–1.6 Ma, after which accumulation dramatically dropped to low rates until a small rise in the Late Pleistocene, that is also seen in the Bengal Fan. The two major changes seen in both fans thus took place at 9.5–8.3 Ma and 5.5–5.2 Ma, suggesting a common mechanism. We now explore if these changes can be linked with any obvious climatic events.

4.1 Influence of Climate

Following the end of the Middle Miocene climatic optimum (a period of relative warmth from 18–14 Ma), the deep-marine composite isotope compilation shows that the $\delta^{18}O$ record was characterised by a series of incremental steps at ~14.6, 13.9, 13.1, 10.6, 9.9, and 9.0 Ma, which have been attributed to progressive deep-water (high-latitude) cooling and/or glaciation (Holbourn *et al*., 2013). The earlier part of this step-wise deterioration in global climate therefore includes the Nicobar Fan, with the so-called Late Miocene "*Carbonate Crash*" at ~11–9 Ma (Lyle *et al*., 2008). A high-resolution benthic isotope record, combined with paired mixed-layer isotope and Mg/Ca-derived temperature data by Holbourn *et al*. (2018) show that a long-term cooling trend was synchronous with the intensification of the Asian winter monsoon and strengthening of the biological pump from ~7–5.5 Ma. The climate shift occurred at the end of a decrease in global $\delta^{13}C$, suggesting that changes in the carbon cycle involving the terrestrial and deep-ocean carbon reservoirs were likely instrumental in driving late Miocene climate cooling.

The start of cooler climate conditions culminated with ephemeral Northern Hemisphere glaciations between 6.0–5.5 Ma (*ibid*.). From the above discussion, we conclude that although there are significant changes in global climate that occurred during the accumulation of the Nicobar Fan, none appear to uniquely bracket this time interval from ~9.5 Ma. This suggests another more local primary causal process.

The South Asian (Indian) monsoon would have had the most influence on fan sediment source areas, although the East Asian monsoon would have impacted the easternmost region including the syntaxis (Namche Barwa). The relationship between annual rainfall and its temporal distribution and erosion as a driver for increased sediment supply (Snyder *et al*., 2003) implies that a stronger monsoon would generate increased physical erosion, fluvial transport and, therefore, lead to increased sediment accumulation rates in the submarine fans. At the present-day, the summer monsoon accounts for ~70% of annual rainfall in all catchments draining into the Bay of Bengal, but due to orographic forcing it focuses precipitation on the southern edge of the Lesser and Greater Himalayan Sequences of the Himalaya. The high- elevation, high- relief, and usually dry areas, are only affected by stronger monsoons and significant precipitation only occurs in the eastern syntaxial region during the winter season (Bookhagen and Burbank, 2010).

The intensity of the South Asian monsoon has been linked to the growth of the Himalaya, especially in the Miocene (Clift *et al*., 2008), and the most significant changes in monsoon intensity took place in the middle Miocene, at ~12.9 Ma, when the monsoon wind system develop in strength and intensity similar to the present conditions (Betzler *et al.*, 2016). Proxy data indicate that from 11 Ma the summer monsoon was weak but had intensified across South and East Asia by 7 Ma (Wan *et al*., 2007; Gupta *et al*., 2015). However, when the summer monsoon was weaker the winter monsoon would have been stronger and Gupta *et al*. (2015) noted that higher sediment accumulation rates seen in the Himalayan foreland (Siwaliks) from 11–7 Ma were probably linked to winter precipitation during strong Westerlies when summer monsoon winds were weaker. From ~7 Ma the long-term global cooling trend appears to have coincided with intensification of the Asian winter monsoon recorded by a long-term trend toward heavier benthic **δ**^{18}O maxima (Zachos *et al*., 2001). The most intense maxima peaked between 5.8–5.5 Ma before reversing in the Pliocene (Holbourn *et al*. 2018).

Stronger winter monsoons in the Miocene means that erosion would tend to be more concentrated on the upper slopes and the eastern syntaxial region, hence fan provenance should be biased towards these areas and that, over time, contributions from these sources should decrease as the summer monsoon strengthened. However, no obvious trend linked to monsoon changes is apparent within the two fan datasets. Bengal Fan thermochronological data (Najman *et al*., 2019) record constant lag-times between ~12–5 Ma associated with steady erosion of the GHS and syntaxial antiform plus a significant component of the THS, but there is also a constant and significant presence of LHS material. The proportions of material from the various Himalayan units (i.e., GHS, THS and LHS) does not change until after 4 Ma, post peak summer monsoon strength at ~5.5 Ma. After this time there is a significant increase in zircons with ages < 300 Ma, and thermochronometry data record short lag-times (Blum *et al*., 2018; Najman *et al*., 2019) diagnostic of rapid exhumation of the eastern syntaxis (Najman *et al*., 2019). Whilst inception of rapid syntaxial exhumation is considered to have started between 7–5 Ma (Bracciali *et al*., 2016; Lang *et al*., 2016), extremely rapid exhumation rates have only been sustained in the Namche Barwa Syntaxis region since 5 Ma (Lang *et al*., 2016). At the present-day, the syntaxis region is noteworthy as a major source of sediment entering the Brahmaputra River system, as indicated by the sediment geochemistry, petrography, and thermochronology data from the Brahmaputra River and its tributaries that suggest 35–70% of the sediment flux of the Brahmaputra River were sourced in the Namche Barwa Syntaxis (Garzanti *et al*., 2004; Singh and France-Lanord, 2002; Stewart *et al*., 2008; Gemigani *et al*., 2018). By contrast, Nicobar Fan samples record constant contributions from the GHS and THS, but LHS material is not always present. Further, in the Nicobar Fan no evidence such as zircon ages < 10 Ma, was found to support significant input from the rapidly exhuming Namche Barwa massif of the eastern syntaxis.

Sediment accumulation in both fans reached their acme between ~9.5–8 Ma similar to major sedimentation in the Himalayan foreland that has been associated with a strong winter monsoon. It may be that climate has influenced MARS in both fan systems. However, post 9 Ma MARS vary between the two fans and changes in sediment provenance do not show a close correspondence to the increase in monsoon intensity that took place between 11–5 Ma or its subsequent weakening. This suggests differences in fan accumulation rates and provenance wss due to other primary causal processes.

4.2 Tectonics

From the above discussion, distinct changes in sediment accumulation that is common in both fans, occurred between 9.5–8.3 Ma (peak MARs) and 5.5–5.2 Ma (sharp drop in MARs). Similarly, both fans share a change in provenance between 5–3 Ma recorded by thermochronometry data that show a switch to rapid exhumation in the Bengal Fan source and a significant slow down in the Nicobar Fan sources (Fig. 8). This change coincided with low rates of accumulation in the Bengal Fan and a marked increase in the Nicobar Fan between 3.8–1.7 Ma.

Perhaps the most important development was a change in the path of the paleo-Brahmaputra River, whereby prior to ~5 Ma the paleo-Brahmaputra River flowed directly south (Fig. 9; Najman *et al*. 2012; Govin *et al*. 2018) although from the late Miocene it would also have been pushed westwards by the expanding Indo–Burma wedge that also folded and exposed earlier sediments deposited in the foreland and remnant ocean basin including the Surma Basin (Najman *et al*. 2012; Betka *et al*., 2018). The Indo–Burma wedge is a thin-skinned fold-thrust belt formed by oblique convergence and accretion of sediments of the Ganges–Brahmaputra Delta (GBD) on the Indian plate with the Shan Plateau (Betka *et al*., 2018). The frontal fold-belt (Chittagong Hill

Tracts) records ongoing deformation of Paleogene – present Himalayan sourced fluvial-deltaic sedimentary rocks of the GBD (Najman *et al*., 2012). These include the late Eocene to early Miocene Barail Formation and, in the outermost belt, the Miocene shallow-marine deposits of the Surma Group, overlain by Miocene–Pliocene Tipam Group fluvial deposits, and Pliocene–Quaternary Dupi Tila Group fluvial and alluvial deposits (Najman *et al*., 2012). These have been folded into a series of fault-cored antiforms separated by wide and low-relief synclinal valleys and were sourced from the Himalaya with a minor arc-derived component from either the "Trans-Himalaya" or recycled from the arc-derived Paleogene Indo–Burman Ranges (Allen *et al*., 2008; Najman *et al*., 2012). Most of the deformation of this outer belt took place between 8–2 Ma based on zircon thermochronometry which limits deformation to < 8 Ma (Betka *et al*., 2018) and onlaps across a latest Pliocene marker bed on a submarine anticline that dates deformation of the frontal part of the wedge to ~2 Ma (Maurin and Rangin, 2009).

The significance of the timing of the westward encroachment of the fold belt, which is also seen in seismic mapping across the Surma Basin (Najman *et al*., 2012), is that it occurred at the same time as the uplift of the Shillong Plateau at 5.2–4.9 Ma (Govin *et al*., 2018). This led to a diversion of the paleo-Brahmaputra River westwards around the Shillong Plateau producing an axial, east to west, route along strike of the mountain front before turning to drain southwards (Govin *et al*., 2018). This development is constrained by fluvial deposits along the Dungsam Chu (Trans-Himalayan) foreland section of eastern Bhutan that show arrival of Trans-Himalayan (Cretaceous–Eocene zircon U–Pb ages) detritus from ~5 Ma onwards (Govin *et al*., 2018). Although Brahamputra River material now routed west of the Shillong Plateau, a southerly drainage also remained open to the east of the plateau until ~2 Ma when westward encroachment of the fold belt reached the margins of the Shillong Plateau. Evidence for this can be seen on seismic lines, and provenance of the Tipam Formation that was later recycled into the Dupa Tila Group (Najman *et al*., 2012). Neogene deposits of the Surma Basin do not record evidence of the rise and erosion of the eastern syntaxis domal pop-up until the late Pliocene–Pleistocene

(Bracciali *et al*., 2016) which is the time by which the southerly drainage east of the plateau had become closed. This explains why the Nicobar Fan samples do not contain zircon U–Pb ages diagnostic of the syntaxis region (ages <10 Ma), whereas the Bengal Fan samples do.

The onset of major river diversions at ~5 Ma coincided with a marked drop in MARS seen in both fans (Fig. 8). However, by 4 Ma accumulation rates in the Nicobar Fan increased again until ~2 Ma when there was another marked drop in accumulation rates that remained low thereafter. By contrast, the Bengal Fan accumulation rates remained low from ~5–0.5 Ma, after which there was a small increase. McNeill *et al*. (2017b) suggested the drop from ~2 Ma, supported the hypothesis that impingement of the NinetyEast Ridge on the Sunda Trench diverted the primary flux west of the ridge along with a concomitant rise in mid–late Pleistocene accumulation rates on the Bengal Fan (e.g., France-Lanord *et al*., 2016). However, as discussed above, a westward re-routing of the Brahmaputra River may also have played a role leading up to final collision of the ridge with the subduction zone that blocked sediment supply from the north (Curray and Moore, 1974).

Whilst the MAR data and detrital zircon U–Pb data suggest changes related to re-organisation of river routing to the fans, the detrital AFT show a constant behaviour in terms of apatite sources until 2 Ma, after which the data suggest a modest slowdown. The main age trend seen in the lag-time plot of figure 7 reflects a constant supply from a source area undergoing steady erosion through time. The short lag-time rules out significant intermediate storage and mixing. The source of apatites is indicated by unreset Siwalik foreland sediments in the Arunachal Pradesh, eastern Bhutan, and Nepal. Here, sands of comparable deposition ages to Nicobar Fan samples yielded identical AFT ages (Table 1) and lag times (Fig. 7). In the Arunachal Pradesh sands, with depositional ages between 0–2 Ma, the dominant population of AFT ages range from 2.9±0.8 Ma to 4.0±0.9 Ma with a secondary population between 7–15 Ma (Chirouze *et al*., 2013). Similar ages are seen to the west in the foreland of Eastern Bhutan. Here, most dominant populations of unreset apatites record AFT ages between from 3.6 ± 0.8 Ma (youngest) up to 6.9±1.2 Ma (8 Ma sample) and secondary populations from 15–10 Ma (Coutand *et al*., 2016). By contrast, modern bedrock AFT ages from the Shillong Plateau are older, ranging from 12.6–8.6 Ma and up to 101 Ma (Biswas, 2007), which rules out this block as a major sediment source for Nicobar Fan apatites.

4.3 Implications for sediment supply

The Nicobar Fan and Bengal Fan can be considered as the respective eastern and western parts of an integrated submarine-fan system. Their constituent sediments have the same provenance, whether delivered by the eastern or western routes from the Brahmaputra River. At ~2 Ma, the eastern drainage route to the Nicobar Fan became closed to direct input from the Ganges-Brahmaputra system, at which time the MARS in Nicobar Fan significantly decreased.

The earliest onset of high MARs in the Bengal Fan occurred at ~14–13.5 Ma, with a switch to the Nicobar Fan at ~9.5 Ma (Fig. 9). The earliest high MARs in the Bengal Fan are broadly consistent with the observed rapid increase in seawater $^{187}Os/^{188}Os$ and decrease in seawater $^{87}Sr/^{86}Sr$ in the mid to late Miocene at ~16–11 Ma, which we interpret to reflect rapid thrust belt advance and exhumation of the outer Lesser Himalaya (Colleps *et al*., 2018). The earliest high MARs in the Nicobar Fan do not demand a similar tectonic explanation in the Himalaya and other associated northern source areas for sediment supply via the Ganges–Brahmaputra drainage basin. The MARs most likely reflect an autocyclic shift from the importance of sediment routing in submarine channel systems to the west of the NinetyEast Ridge (Bengal Fan) to an eastern predominance (Nicobar Fan), i.e., switching to a dominance of fan deposition on the Nicobar Fan. However, an inspection of the MARs for the both the Bengal and Nicobar fans shows that the high MARs in the Bengal Fan do not show a substantial decrease until ~8.5–8 Ma, at least 1 Myr after the dramatic increase in the Nicobar Fan (Fig. 9), suggesting that other contributory factors, (e.g., tectonic), maintained the overall high sediment flux. For example, a comprehensive magnetostratigraphic and sedimentologic study of the Dati Basin in the northern Himalaya Mountains by Zhang *et al*. (2019) recorded pulses of accelerated tectonic uplift and erosion of the Himalaya Mountains at ~10.0 Ma, ~3.0 Ma, and at ~1.7 Ma.

At ~5 Ma, a drop in MARs is observed in both the Nicobar Fan and Bengal fans. Also, at ~5 Ma, there was a change in river drainage to west of uplifting Shillong Plateau, but as seen in the provenance (Tipam Formation; Shrivastava *et al*., 1974; Sahoo and Gogoi, 2009; Sarma and Chutia, 2013). Drainage remained open to the east of the Shillong Plateau.

At ~4–3.5 Ma, an increase in MARs in recorded in the Nicobar Fan, but the Bengal Fan MARs remained low. These younger increased MARs might be related to accelerated erosion in the Namche Barwa syntaxis with hysteresis effects. The inception of rapid syntaxial exhumation started between 7–5 Ma (Bracciali *et al*., 2016) and extremely rapid exhumation rates have been sustained in the Namche Barwa region since ~5 Ma (Lang *et al*., 2016). The syntaxis region is noteworthy as a major source of sediment entering the Brahmaputra based on studies using sediment geochemistry, petrography, and thermochronology data from the Brahmaputra and its tributaries that estimate 35–70% of the sediment flux of the Brahmaputra was sourced Namche Barwa (Enkelmann *et al*., 2011; Garzanti *et al*., 2004; Gemigani *et al*., 2018; Singh and France-Lanord, 2002; Stewart *et al*., 2008). Note that the Neogene Surma Basin does not record evidence of the rise and erosion of the domal pop-up until latest Pliocene–Pleistocene time (Bracciali *et al*., 2016) and that Nicobar Fan samples do not contain zircon U–Pb ages diagnostic of this region (ages < 10 Ma), whereas Bengal Fan samples do.

Since ~10 Ma, global sea level has generally fallen (Miller *et al*., 2005), thereby decreasing accommodation on the shelf, and thus amplifying the processes driving sediment southward into the deep Indian Ocean. A fundamental question, however, is the reason for the submarine routing system to favour the Nicobar Fan over the Bengal Fan since ~9.5–2 Ma.

5. Conclusions

U–Pb age spectra of detrital zircons, sand petrography, and heavy-mineral analysis confirm that the Nicobar Fan was a major sink for Himalaya-derived material. Our data show the Nicobar Fan sands are similar but not identical to Bengal Fan sands, such that the Nicobar Fan sands lack young zircons derived from the eastern Himalayan syntaxis. These are present in Bengal Fan sands deposited after < 3 Ma. This timing coincides with the group of Bengal Fan samples that show closest affinity to the Brahmaputra River that re-routed at that time to a modern configuration. The Nicobar Fan samples show AFT ages consistent with erosion of the frontal Himalaya and/or contemporaneous erosion of similar age foreland sediments.

The petrographic data suggests that supply from the metamorphic axial core of the Himalayan range (GHS) has increased in the last 5.5 Ma. The down-core decrease in heavy-mineral concentration and the proportion of transparent heavy minerals relative to the heavy fraction also may be effects of intrastratal solution and grain size. The coarsening-upward trend indicated by the samples explains the upward decrease in the epidote/garnet ratio.

Apatite fission track data shows that source area exhumation, routing and burial were extremely rapid from ~8–3 Ma. This broadly corresponds to a time of fan re-organisation. We interpret this latter signal as due to both rapid rapid exhumation in the source area and lowered mean sea level during global cooling. The more distant Investigator Fan and the thick accretionary prism of the Sunda subduction zone of the easternmost Indian Ocean also contain significant amounts of Oligocene-Miocene Himalaya-derived material.

We conclude that although there are significant changes in global climate that occurred during the accumulation of the Nicobar Fan, none appear to uniquely bracket the time interval from ~9.5 Ma when high and sustained MARs began. Similar arguments can be made for the Bengal Fan. Since ~5 Ma, tectonically driven changes in the river network most influenced fan sedimentation and provenance. These changes can account for the main differences seen between the Bengal and Nicobar Fan, that were enhanced by the global deterioration in climate and associated eustatic sea-level falls, to strengthen the sediment flux to the Nicobar and Bengal fans.

References

Allen, R., Najman, Y., Carter, A., Barfod, D., Bickle, M.J., Chapman, H.J., Garzanti, E., Vezzoli, G., Andò, S. and Parrish, R. 2008. Provenance of the Tertiary sedimentary rocks of the Indo-Burman Ranges, Burma (Myanmar): Burman arc or Himalayan-derived? *Journal of the Geological Society London*, **165**, 1045–1057.

Andò, S., Garzanti, E., Padoan, M. and Limonta, M. 2012. Corrosion of heavy minerals during weathering and diagenesis: a catalog for optical analysis. *Sedimentary Geology*, **280**, 165-178.

Betka, P.M., Seeber, L., Thomson, S.N., Steckler, M.S., Sincavage, R. and Zoramthara, C. 2018. Slip-partitioning above a shallow, weak décollement beneath the Indo-Burman accretionary prism. *Earth and Planetary Science Letters*, **503**, 17–28.

Betzler, C. *et al*. 2016. The abrupt onset of the modern South Asian Monsoon winds. *Science Report*, **6**, 29838; doi: 10.1038/srep29838.

Biswas, S., Coutand, I., Grujic, D., Hager, C., Stockli, D. and Grasemann, B., 2007. Exhumation and uplift of the Shillong Plateau and its influence on the eastern Himalayas: new constraints from apatite and zircon (U–Th–[Sm])/He and apatite fission track analyses. *Tectonics*, **26**, TC6013.

Bracciali, L., Parrish, R.R., Najman, Y., Smye, A.J., Carter, A. and Wijbrans, J.R. 2016. Plio-Pleistocene exhumation of the eastern Himalayan syntaxis and its domal 'pop-up'. *Earth Science Reviews*, **160**, 350–385.

Blum, M., Kimberly Rogers, K., Gleason, J., Najman, Y., Cruz, J. and Fox, L. 2018. Allogenic and autogenic signals in the stratigraphic record of the deep-sea Bengal Fan. *Nature Scientific Reports*, **8**, 7973. doi:10.1038/s41598-018-25819-5.

Bookhagen, B. and Burbank, D.W. 2010. Toward a complete Himalayan hydrological budget: Spatiotemporal distribution of snowmelt and rainfall and their impact on river discharge. *Journal of Geophysical Research*, **115**, F03019, doi:10.1029/2009JF001426

Booth, A.L., Zeitler, P.K., Kidd, W.S., Wooden, J., Liu, Y., Idleman, B., Hren, M. and Chamberlain, C.P. 2004. U-Pb Zircon constraints on the tectonic evolution of southeastern Tibet, Namche Barwa area. *American Journal of Science,* **304**, 889–929.

Campbell, I.H., Reiners, P.W., Allen, C.M., Nicolescu, S. and Upadhyay, R. 2005. He–Pb double dating of detrital zircons from the Ganges and Indus Rivers: Implication for quantifying sediment recycling and provenance studies. *Earth and Planetary Science Letters*, **237**, 402–432.

Chirouze, F., Huyghe, P., van der Beek, P., Chauvel, C., Chakraborty, T., Dupont-Nivet, G. and Bernet, M. 2013. Tectonics, exhumation, and drainage evolution of the eastern Himalaya since13 Ma from detrital geochemistry and thermochronology, Kameng River, Section, Arunachal Pradesh. *Geological Society of America Bulletin*, **125**, 523–538.

Clift, P.D., Hodges, K.V., Heslop, D., Hannigan, R., van Long, H. and Calves, G. 2008. Correlation of Himalayan exhumation rates and Asian monsoon intensity. *Nature Geoscience*, 1, 875–880.

Colleps, C.L., Ryan McKenzie, N., Stockli, D.F., Hughes, N.C., Singh, B.P., Webb, A.A.G., Myrow, P.M., Planavsky, N.J. and Horton, B.K. 2018. Zircon (U-Th)/He Thermochronometric constraints on Himalayan thrust belt exhumation, bedrock weathering, and Cenozoic seawater chemistry. *Geochemistry, Geophysics, Geosystems*, **19**, 257–271.

Coutand, I., Barrier, L., Govin, G., Grujic, D., Hoorn, C., Dupont-Nivet, G. and Najman, Y. 2016. Late Miocene-Pleistocene evolution of India-Eurasia convergence partitioning between the Bhutan Himalaya and the Shillong Plateau: New evidences from foreland basin deposits along the Dungsam Chu section, eastern Bhutan. *Tectonics*, **35**, 2963–2994.

Curray, J.R. 1991. Possible greenschist metamorphism at the base of a 22-km sedimentary section, Bay of Bengal. *Geology*, **19**, 1097–1100.

Curray, J.R. and Moore, D.G. 1971. Growth of the Bengal deep-sea fan and denudation in the Himalayas. *Geological Society American Bulletin*, **82**, 563–572.

DeCelles, P.G., Gehrels, G.E., Quade, J., Ojha, T.P., Kapp, P.A. and Upreti, B.N. 1998. Neogene foreland basin deposits, erosional unroofing, and the kinematic history of the Himalayan fold-thrust belt, western Nepal. *Geological Society of America Bulletin*, *110*, 2-21.

France-Lanord, C., Spiess, V., Klaus, A. and the Expedition 354 Scientists 2016. *Neogene and late Paleogene record of Himalayan orogeny and climate: a transect across the Middle Bengal Fan. International Ocean Discovery Program Expedition*, **354,** Preliminary Report, Bengal Fan.

Galbraith, R.F. 2005. Statistics for Fission Track Analysis. Interdisciplinary Statistics Series, 224 pp. Chapman and Hall/CRC.

Garzanti, E. 2016. From static to dynamic provenance analysis - sedimentary petrology upgraded. *Sedimentary Geology*, **336**, 3–13.

Garzanti, E., Vezzoli, G., Andò, S., France-Lanord, C., Singh, S.K. and Foster, G. 2004. Sand petrology and focused erosion in collision orogens: the Brahmaputra case. *Earth and Planetary Science Letters*, **220**, 157–174.

Garzanti, E., Andó, S., France-Lanord, C., Vezzoli, G. and Najman, Y. 2010. Mineralogical and chemical variability of fluvial sediments. 1. Bedload sand (Ganga-Brahmaputra, Bangladesh). *Earth and Planetary Science Letters*, **299**, 368–381.

Garzanti, E. 2019. The Himalayan Foreland Basin from collision onset to the present: a sedimentary–petrology perspective. *In*: Treloar, P.J. and Searle, M.P. (eds), *Himalayan Tectonics: A Modern Synthesis*. Geological Society, London, Special Publications, **483**, 65–122.

Geersen, J., Bull, J.M., McNeill, L.C., Henstock, T.J., Gaedicke, C., Chamot-Rooke, N. and Delescluse, M. 2015. Pervasive deformation of an oceanic plate and relationship to large >MW8 intraplate earthquakes: The northern Wharton Basin, Indian Ocean. *Geology*, **43**, 359–362.

Gehrels, G., Kapp, P., DeCelles, P., Pullen, A., Blakey, R., Weislogel, A., Ding, L., Guynn, J., Martin, A., McQuarrie, N. and Yin, A. 2011. Detrital zircon geochronology of pre-Tertiary strata in the Tibetan-Himalayan orogen. *Tectonics*, **30**, 1944–1994.

Gemignani, L., van der Beek, P.A. Braun, J., Najman, Y., Bernet, M., Garzanti, E. and Wijbrans, J.R. 2018. Downstream evolution of the thermochronologic age signal in the Brahmaputra catchment (eastern Himalaya): Implications for the detrital record of erosion. *Earth and Planetary Science Letters*, **499**, 48–61.

Govin, G., Najman, Y., Dupont-Nivet, G., Millar, I., van der Beek, P., Huyghe, P., O'Sullivan, P., Mark, C. and Vögell, N. 2018. The tectonics and paleo-drainage of the easternmost Himalaya (Arunachal Pradesh, India) recorded in the Siwalik rocks of the foreland basin. *American Journal of Science*, **318**, 764–798.

Gupta, K., Yuvaraja, A., Prakasam, M., Clemens, S. C. and Velu, A. 2015. Evolution of the South Asian monsoon wind system since the late Middle Miocene. *Palaeogeography., Palaeoclimatology*. *Palaeoecology*. **438**, 160–167.

Heroy, D.C., Kuehl, S.A. and Goodbred, S.L. 2003. Mineralogy of the Ganges and Brahmaputra Rivers: implications for river switching and Late Quaternary climate change. *Sedimentary Geology*, **155**, 343–359.

Holbourn, A., Kuhnt, W., Clemens, S., Prell, W. and Andersen, N. 2013. Middle to late Miocene stepwise climate cooling: evidence from a high-resolution deep water isotope curve spanning 8 million years. *Paleoceanography*, **28**, 688–699.

Holbourn, A.E., Kuhnt, W., Clemens, S.C., Kochmann, K.G.D., Jöhnck, J., Lubbers, J. and Andersen, N. 2018. Late Miocene climate cooling and intensification of southeast Asian winter monsoon. *Nature Communications*, doi: 10.1038/s41467-018-03950-1.

Ingersoll, R.V. and Suczek, C.A. 1979. Petrology and provenance of Neogene sand from Nicobar and Bangal fans, Deep Sea Drilling Project Sites 211 and 218. *Journal of Sedimentary Petrology*, **49**, 1217–1228.

Jena B., Kurian, P.J. and Avinash, K. 2016. Morphology of submarine channel-levee systems in the eastern Bay of Bengal near Andaman region. *Journal of Coastal Conservation*, **20**, 211–220.

Ji, W-Q., Wu, F-Y., Liu, X-C., Liu, Z-C., Zhang, C., Liu, T., Wang, J-G. and Paterson, S.R. 2019. Pervasive Miocene melting of thickened crust from the Lhasa terrane to Himalaya, southern Tibet and its constraint on generation of Himalayan leucogranite. *Geochimica et Cosmochimica Acta*, doi.org/10.1016/j.gca.2019.07.048

Lang, K.A., Huntington, K.W., Burmester, R. and Housen, B. 2016. Rapid exhumation of the eastern Himalayan syntaxis since the late Miocene. *Geological Society of America Bulletin*, **128**, 1403–1422. Doi:10.1130/B31419

Limonta, M., Resentini, A., Carter, A., Bandopadhyay, P.C. and Garzanti, E. 2017. Provenance of Oligocene Andaman sandstones (Andaman–Nicobar Islands): Ganga–Brahmaputra or Irrawaddy derived? *In*: Bandopadhyay, P.C. and Carter, A. (eds), *The Andaman–Nicobar Accretionary Ridge: Geology, Tectonics and Hazards*, 143–154. Geological Society London Memoir, **47**.

Lyle, M., Barron, J., Bralower, T.J., Huber, M., Lyle, A.O., Ravelo, A.C., Rea, D.K. and Wilson, P.A. 2008. Pacific Ocean and Cenozoic evolution of climate. *Reviews in Geophysics*, **46**, RG2002, doi:10.1029/2005RG000190.

Maurin, T. and Rangin, C. 2009. Structure and kinematics of the Indo-Burmese Wedge: Recent and fast growth of the outer wedge. *Tectonics*, **28**, TC2010, doi:10.1029/

McNeill, L.C., Dugan, B., Petronotis, K.E., Backman, J., Bourlange, S., Chemale, F., Chen, W., Colson, T.A., Frederik, M.C.G., Guèrin, G., Hamahashi, M., Henstock, T., House, B.M., Hüpers, A., Jeppson, T.N., Kachovich, S., Kenigsberg, A.R., Kuranaga, M., Kutterolf, S., Milliken, K.L., Mitchison, F.L., Mukoyoshi, H., Nair, N., Owari, S., Pickering, K.T., Pouderoux, H.F.A., Yehua, S., Song, I., Torres, M.E., Vannucchi, P., Vrolijk, P.J., Yang, T. and Zhao, X. 2017a. Expedition 362 methods. *In*: McNeill, L.C., Dugan, B., Petronotis, K.E., and the Expedition 362 Scientists, *Sumatra Subduction Zone. Proceedings of the International Ocean Discovery Program*, **362**, Sumatra Subduction Zone. College Station, TX (International Ocean Discovery Program). https://doi.org/10.14379/iodp.proc.362.102.2017

McNeill, L.C., Dugan, B., Backman, J., Pickering, K.T., Pouderoux, H.F.A., Henstock, T.J., Petronotis, K.E., Carter, A., Chemale, F. Jr., Milliken, K.L., Kutterolf1, S., Mukoyoshi1, H., Chen, W., Kachovich, S., Mitchison, F.L., Bourlange, S., Colson, T.A., Frederik, M.C.G., Gilles Guèrin, G., Hamahashi, M., House, B.M., Hüpers, A., Jeppson, T.N., Kenigsberg, A.R., Kuranaga, M., Nair, N., Owari, S., Shan, Y., Song, I., Torres, M.E., Paola Vannucchi, P., Vrolijk, P.J., Yang, T., Xixi Zhao, X. and Thomas, E. 2017b. Understanding Himalayan erosion and the significance of the Nicobar Fan. *Earth and Planetary Science Letters*, **475**,134–142. doi:10.1016/j.epsl.2017.07.019

Miller, K.G, Kominz, M.A., Browning, J.V., Wright, J.D., Mountain, G.S. and Katz, M.E. 2005. The Phanerozoic record of global sea-level change. *Science*, **310**, 1293–1298.

Mitchell, A., Chung, S.L., Oo, T., Lin, T.H. and Hung, C.H. 2012. Zircon U–Pb ages in

Myanmar: Magmatic–metamorphic events and the closure of a neo–Tethys ocean. *Journal of Asian Earth Sciences*, **56**, 1–23.

Najman, Y. and Garzanti, E. 2000. Reconstructing early Himalayan tectonics evolution and paleogeography from Tertiary foreland basin sedimentary rocks, northern India. *Geological Society of America Bulletin*, **112**, 435–449.

Najman, Y., Bickle, M, BouDagher-Fadel, M., **Carter, A**., Garzanti, E., Paul, M., Wijbrans, J., Willett, E., Oliver, G., Parrish, R., Akhter, H., Allen, R.,. Ando, S., Chisty, E., Reisberg, L. and Vezzoli, G. 2008. The Paleogene record of Himalayan erosion: Bengal Basin, Bangladesh. *Earth and Planetary Science Letters, 273,*1–14.

Najman, Y., Allen, R., Willett, E, Carter, A, Barford, D., Garzanti, E, Wijbrans, J., Bickle, M., Vezzoli, G., Ando, S., Oliver, G and Uddin, M.J. 2012, 'The record of Himalayan erosion preserved in the sedimentary rocks of the Hatia Trough of the Bengal Basin and the Chittagong Hill Tracts, Bangladesh'. *Basin Research*, **24**, 499– 519.

Najman, Y., Mark, C., Barfod, D.N., Carter, A., Parrish, R., Chew, D. and Gemignani, L. 2019. Spatial and temporal trends in exhumation of the Eastern Himalaya and syntaxis as determined from a multitechnique detrital thermochronological study of the Bengal Fan. *Geological Society of America Bulletin*, **131**, 1607–1622.

Pickering, K.T. and Hiscott, R.N. (with contribution by Heard, T.G.) 2016. *Deep Marine Systems: Processes, Deposits, Environments, Tectonic and Sedimentation*. Wiley and American Geophysical Union (AGU), 672 pp. ISBN: 978-1-4051-2578-9.

Pickering, K.T., Pouderoux, H., McNeill, L.C., Backman, J., Chemale, F., Kutterolf, S., Milliken, K., Mukoyoshi, H., Henstock, T.J., Stevens, D.E., Parnell, C. and Dugan, B. 2019. Sedimentology, stratigraphy and architecture of the Nicobar Fan (Bengal–Nicobar Fan System), Indian Ocean: Results from International Ocean Discovery Program Expedition 362. *Sedimentology*, doi: 10.1111/sed.12701.

Robinson, R.A.J., Brezina, C.A., Parrish, R.R., Horstwood, M.S.A., Oo, N.W., Bird, M.I., Thein, M., Walters, A.S., Oliver, G.J.H. and Zaw, K. 2014. Large rivers and Orogens: the evolution of the Yarlung Tsangpo–Irrawaddy system and the eastern Himalayan syntaxis. *Gondwana Research*, **26**, 112–121.

Sahoo, M. and Gogoi, K.D. 2009. Depositional history, processes and mechanism of early Miocene sediments of Upper Assam Basin. *Journal of the Geological Society of India*, **73**, 575–585.

Sarma, J.N. and Chutia, A. 2013. Petrography of sub-surface Tipam Sandstone Formation of a part of Upper Assam Basin, India. *Global Research Analysis*, **2**, 112–113.

Shrivastava, P.K., Ganeshan, S. and Ray, D. 1974. Tipam Group in the Subsurface of Upper Assam Valley, South of Brahmaputra. *Journal of the Geological Society of India*, **15**, 165–181.

Singh, S.K., France-Lanord, C. 2002. Tracing the distribution of erosion in the Brahmaputra watershed from isotopic compositions of stream sediments. *Earth and Planetary Science Letters*, **202**, 645–662.

Snyder, N.P., Whipple, K.X., Tucker, G.E. and Merrits, D.J. 2003. Importance of a stochastic distribution of floods and erosion thresholds in the bedrock river incision problem, *Journal Geophysical Research*, **108**(B2), 2117, doi:10.1029/2001JB001655

Stewart, R.J., Hallet, B., Zeitler, P.K., Malloy, M.A., Allen, C.M. and Trippett, D. 2008. Brahmaputra sediment flux dominated by highly localized rapid erosion from the easternmost Himalaya. *Geology*, **36**, 711–739.

Thiede, R.C. and Ehlers, T.A. 2013. Large spatial and temporal variations in Himalayan denudation. *Earth and Planetary Science Letters*, **371**, 278–293.

Thompson, R.W. 1974. Mineralogy of sands from the Bengal and Nicobar fans, sites 218 and 211, eastern Indian Ocean. *In*: von der Borch, C.C., Sclater, J.G. *et al*. (eds), Initial Reports of the Deep Sea Drilling Project, **22**, 711–713. United States Government Printing Office, Washington, DC.

Vermeesch, P. 2012. On the visualisation of detrital age distributions. *Chemical Geology*, **312-313**, 190–194, doi: 10.1016/j.chemgeo.2012.04.021.

Vermeesch, P. 2013, Multi-sample comparison of detrital age distributions. *Chemical Geology*, **341**, 140– 146.

Wan, S., Li, A., Clift, P.D. and Stuut, J-B.W. 2007. Development of the East Asian monsoon: mineralogical and sedimentologic records in the northern South China Sea since 20 Ma. *Palaeogeography, Palaeoclimatology, Palaeoecology*, **254**, 561–582.

Yokohama, K., Amano, K., Taira, A. and Saito, Y. 1990. Mineralogy of silts from the Bengal Fan. *In*: Cochran, J.R., Stow, D.A.V. *et al*. (eds) Proceedings of the Ocean Drilling Program, Scientific Results, **116**, 59–73. Ocean Drilling Program, College Station, Texas.

Zachos, J.C., Pagani, M., Sloan, L., Thomas, E and Billups, K. 2001. Trends, rhythms, and aberrations in global climate 65 Ma to present. *Science*, **292**, 689–693.

Zhang, W., Zhang, D., Fang, X., Zhang, T., Chen, C. and Yan, M. 2019. New paleomagnetic constraints on rift basin evolution in the northern Himalaya mountains. *Gondwana Research*, **77**, 98–110.

List of figures

Figure 1. Regional map of the Bengal Nicobar and Investigator fans. The map includes the deep-marine sedimentary system with fans separated by ridges, the Ganges–Brahmaputra River system, and relevant DSDP/ODP/IODP drill sites. No identifiable Bengal Fan sediments were found at DSDP Site 213, and DSDP Site 215 shows a hiatus from lower Eocene clay and nannofossil ooze to lower Miocene silty clay, that Curray (1991) interpreted as distal Bengal Fan sediments. DSDP Site 211 has a hiatus from non-fossiliferous clays overlying Maastrichtian to Pliocene strata, again probably distal fan sediments. The Investigator Fan, where Site 211 is located, is called after the Investigator Ridge. Channels recognised on the seafloor are reported after Curray and Moore (1971). Top right inset is a bathymetry map of the seafloor around IODP Expedition 362 sites (modified from Geersen *et al*., 2015); note the presence of well-identified channel heading south. The black box at ~10°N shows the study area of Jena *et al*. (2016) who proved the connection between channel E7 in the Bengal Fan and the Nicobar Channel.

Figure 2. Geology of potential source areas for the sediments in the Nicobar and Bengal submarine fans. Modified after Mitchell *et al*. (2012) and Robinson *et al*. (2014).

Figure 3. Schematic summary of lithostratigraphic units and subunits defined during IODP Expedition 362 in Holes U1480E–U1480G. Drilling in the nearby Hole U1481 recovered core from Units II and III. Sand-prone intervals were defined from a synthesis of the sand-size fraction in recovered cores. Modified from McNeill *et al*. (2017a).

Figure 4. QFL diagram showing the progressive upward change of detrital modes, from feldspatho-litho-quartzose Petrofacies D (grey) and litho-feldspatho-quartzose Petrofacies C (yellow), to quart-rich feldspatho-quartzose Petrofacies B (orange), and eventually feldspatho-quartzose Petrofacies A (red). In Petrofacies D, the grey colour of the symbols becomes darker with depth; conversely, colours become brighter up-section in symbols of other petrofacies. Classification fields are after Garzanti (2016).

Figure 5. Sample detrital zircon U–Pb age distributions plotted as adaptive kernel density estimates (Vermeesch, 2013), comparing data from this study with Bengal Fan dataset of Blum *et al*. (2018) and representative river sands from the Ganges and Brahmaputra rivers.

Figure 6. (**A**) Multidimensional scaling maps (MDS) comparing zircon U–Pb datasets for the Nicobar and Bengal fans, Ganges and Brahmaputra rivers (data from Blum *et al*., 2018). Pink circles show BF, brown Nicobar Fan and blue river samples. Numbers refer to sample age (Ma). Note the branch of Bengal Fan samples that most closely resemble the modern Brahmaputra are all ≤ 3.2 Ma. (**B**) Differences between the Nicobar and Bengal fans highlighted by the red circled area on the MDS plot in 6A is largely due to a higher percentage of young (< 50 Ma) grain ages for samples with a deposition age <4 Ma in the BF samples. (**C**) MDS map comparing fan samples with stratigraphic units of the Surma Basin (yellow) and Pliocene Himalayan foreland sediments (green) from the Dungsam Chu section eastern Bhutan (Govin *et al*., 2018). (**D**) Compares the percentage contributions using the age groups of Blum *et al.* (2018).

Figure 7. Graph showing lag-time relationships between sample depositional age and youngest population of apatite fission track ages for samples from the Nicobar Fan and unreset Siwalik foreland sediments.

Figure 8. Mass accumulation rates (MARs) for IODP sites 1451 (Bengal Fan) and 1480 (Nicobar Fan) from Pickering *et al*. (2019).

Figure 9. Links between submarine-fan MARS and paleogeographic and drainage changes since the late Miocene. Fan reconstructions after McNeill *et al*. (2017) and upper three maps show major river drainage changes adapted from Govin *et al*. (2018), and Najman *et al*. (2012). Arrows link paleogeographic maps with relevant parts of the MAR graph for both the Nicobar and Bengal fans. IBR = Indo-Burman Range; SB = Surma Basin; DC = Dungsam Chu section; NP = Namcha Barwa.

List of tables

Table 1: Summary of AFT results. Samples of similar deposition age shown in italics were combined for age component modelling. Included for comparison are the main provenance ages of unreset Siwalik foreland sediments of comparable deposition age (Chirouz *et al.*, 2013; Coutand *et al*., 2016). Errors on ages are 1sigma.

Figure 1

Click here to download Figure: Fig1_Pickering_et_al 2019.pdf

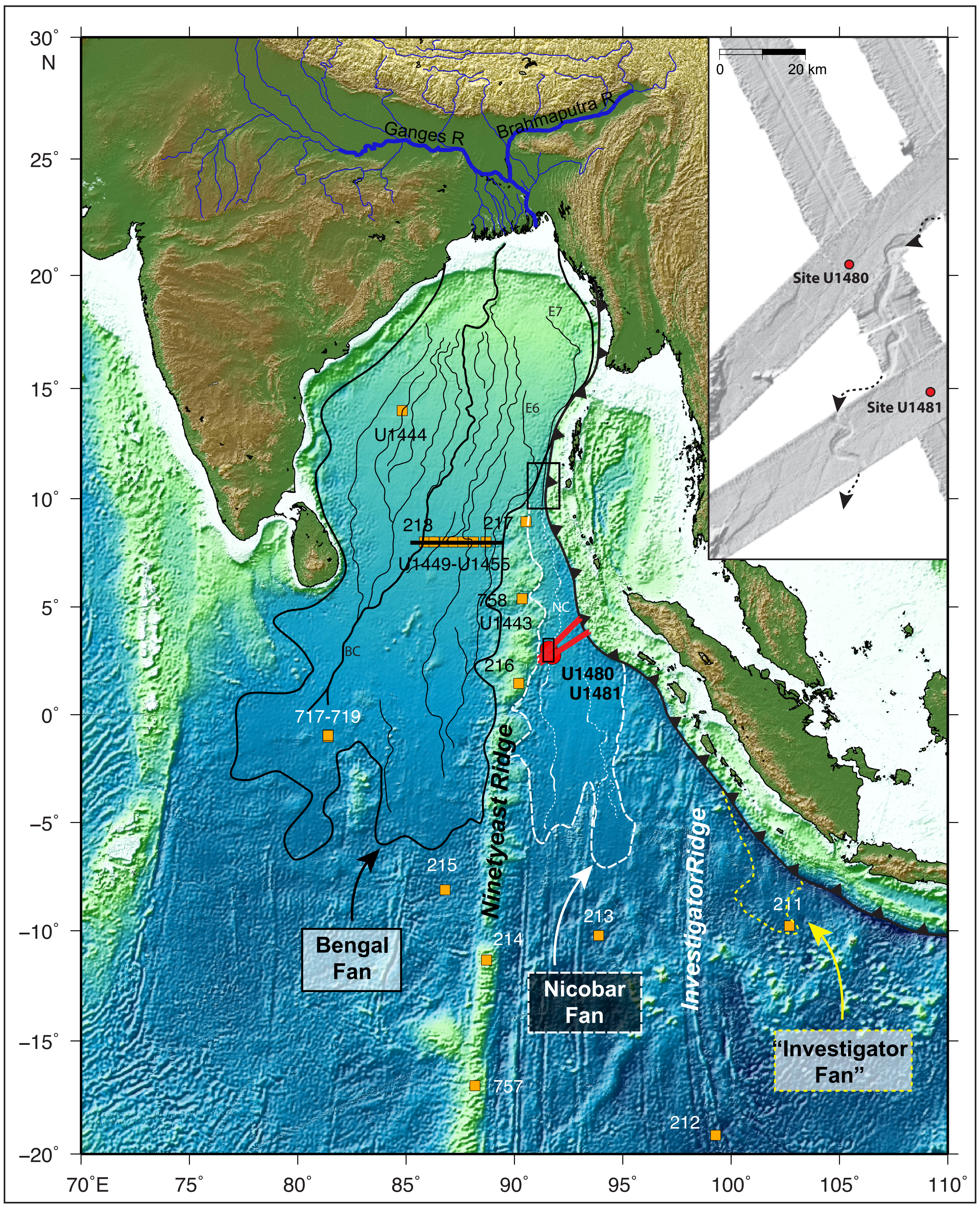

Figure 2

Click here to download Figure: Fig2_Pickering et al.pdf

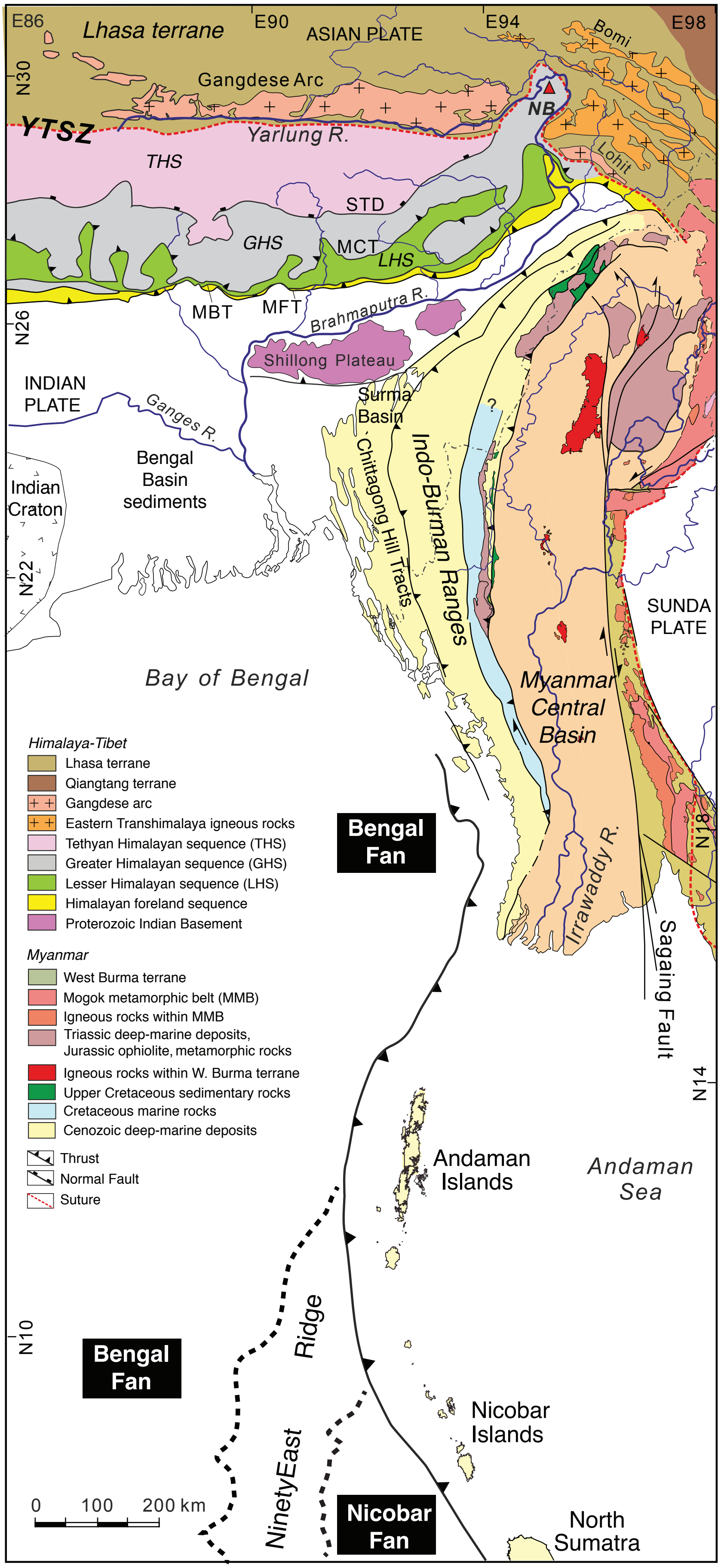

Figure 3
Click here to download Figure: Fig3_Pickering et al.pdf

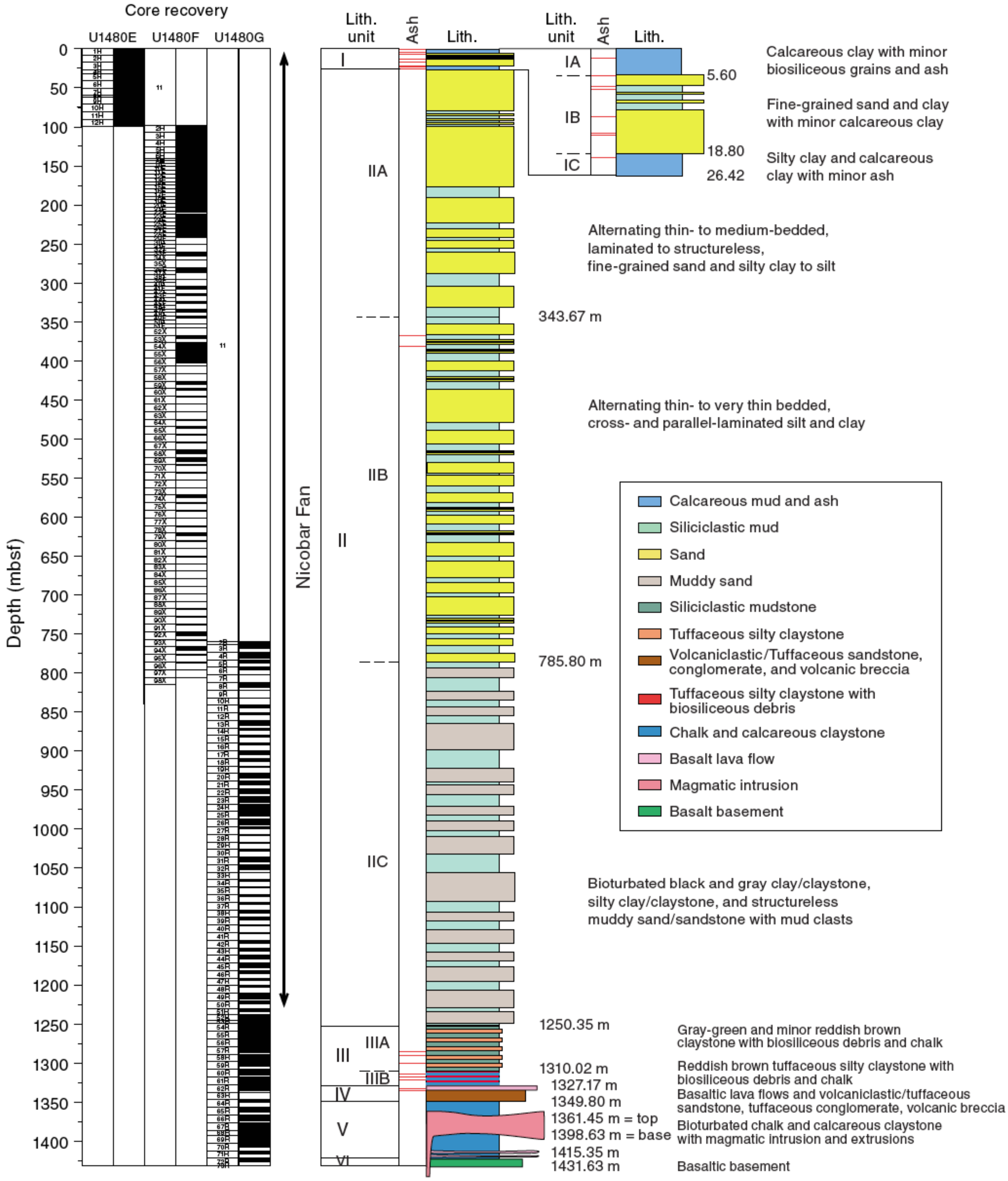

Figure 4

Click here to download Figure: Fig4_Pickering et al.pdf

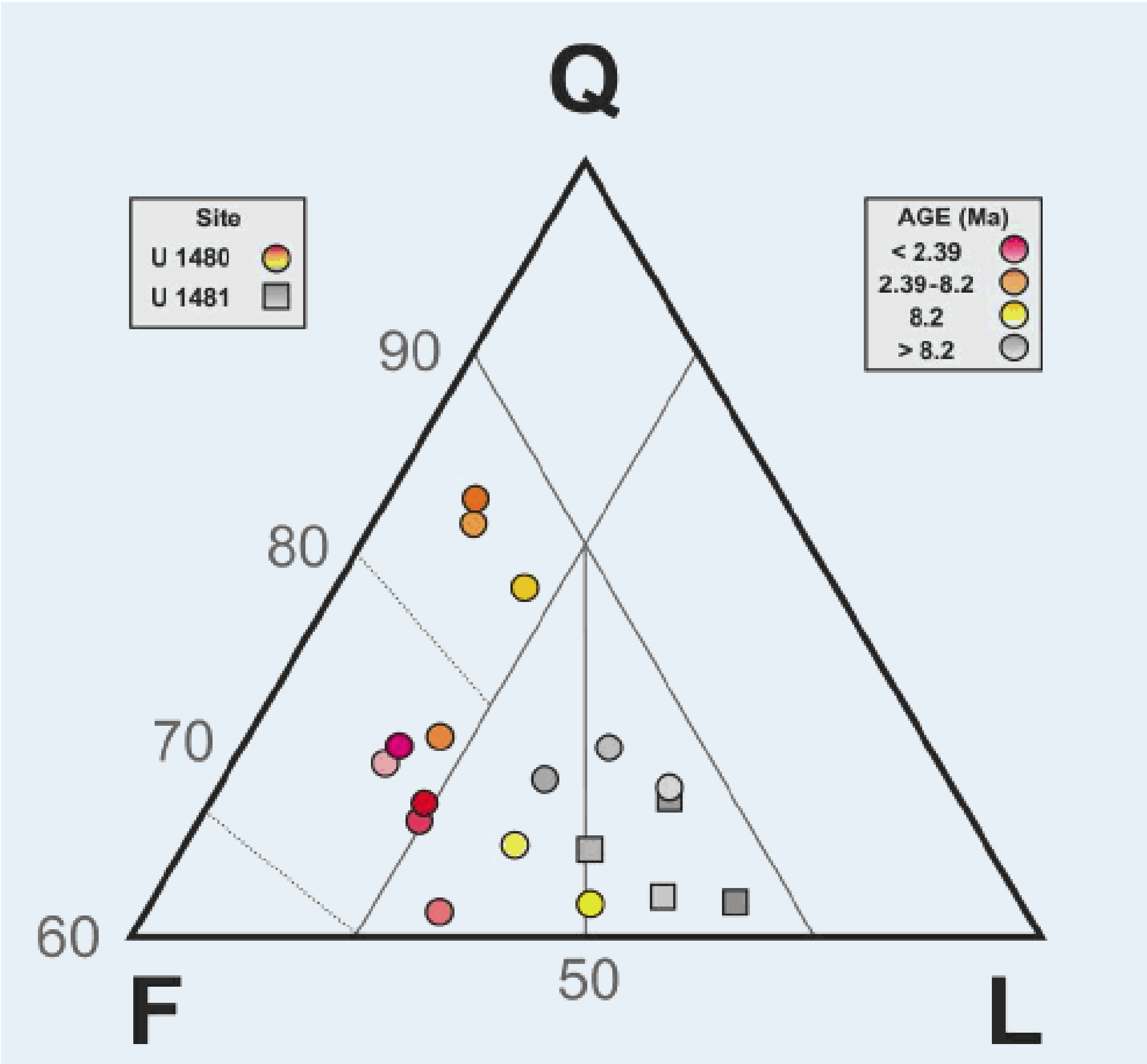

Figure 5

Click here to download Figure: Replacement Fig 5.pdf

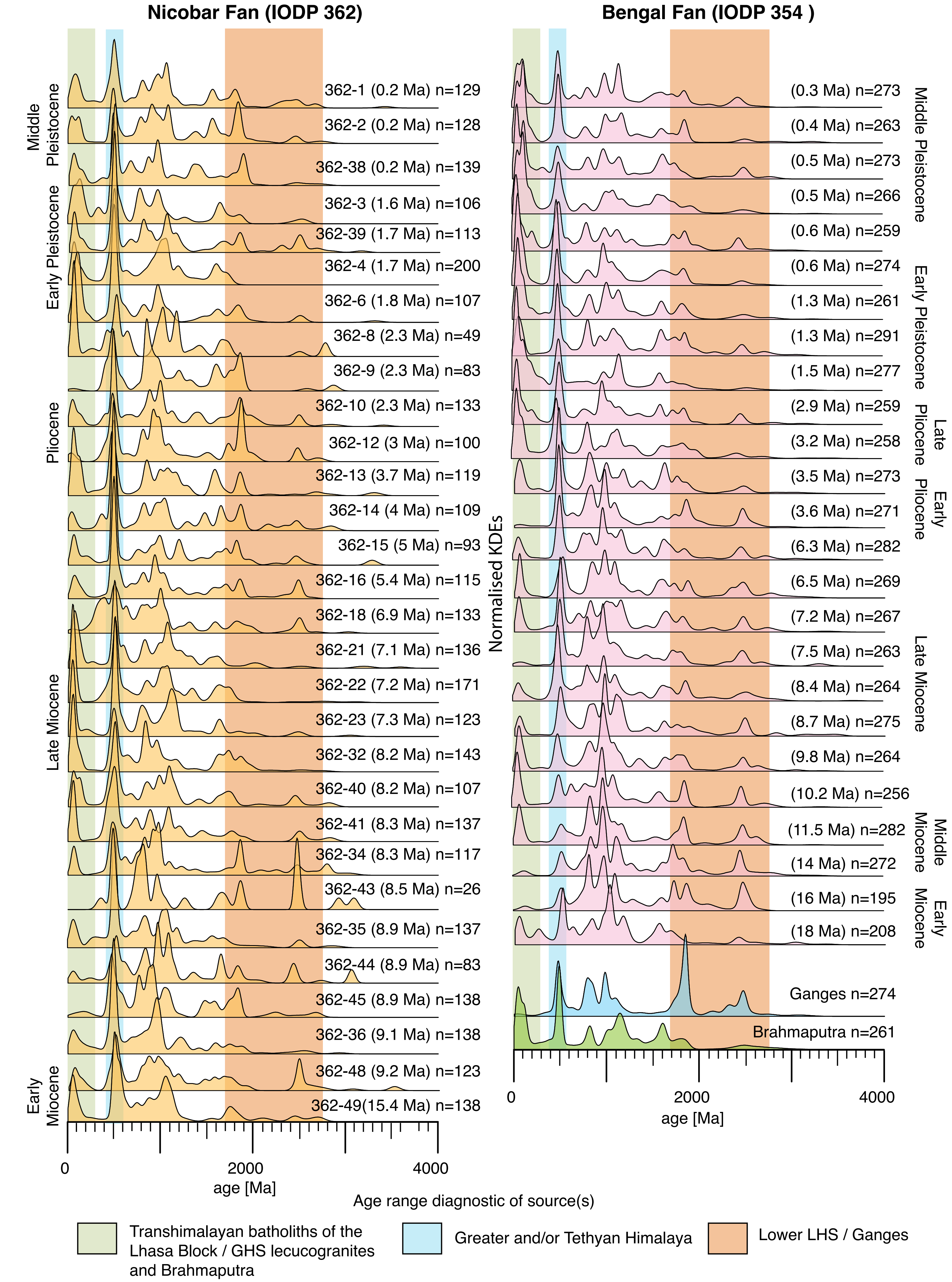

Figure 6

Click here to download Figure: Fig6_Pickering et al.pdf

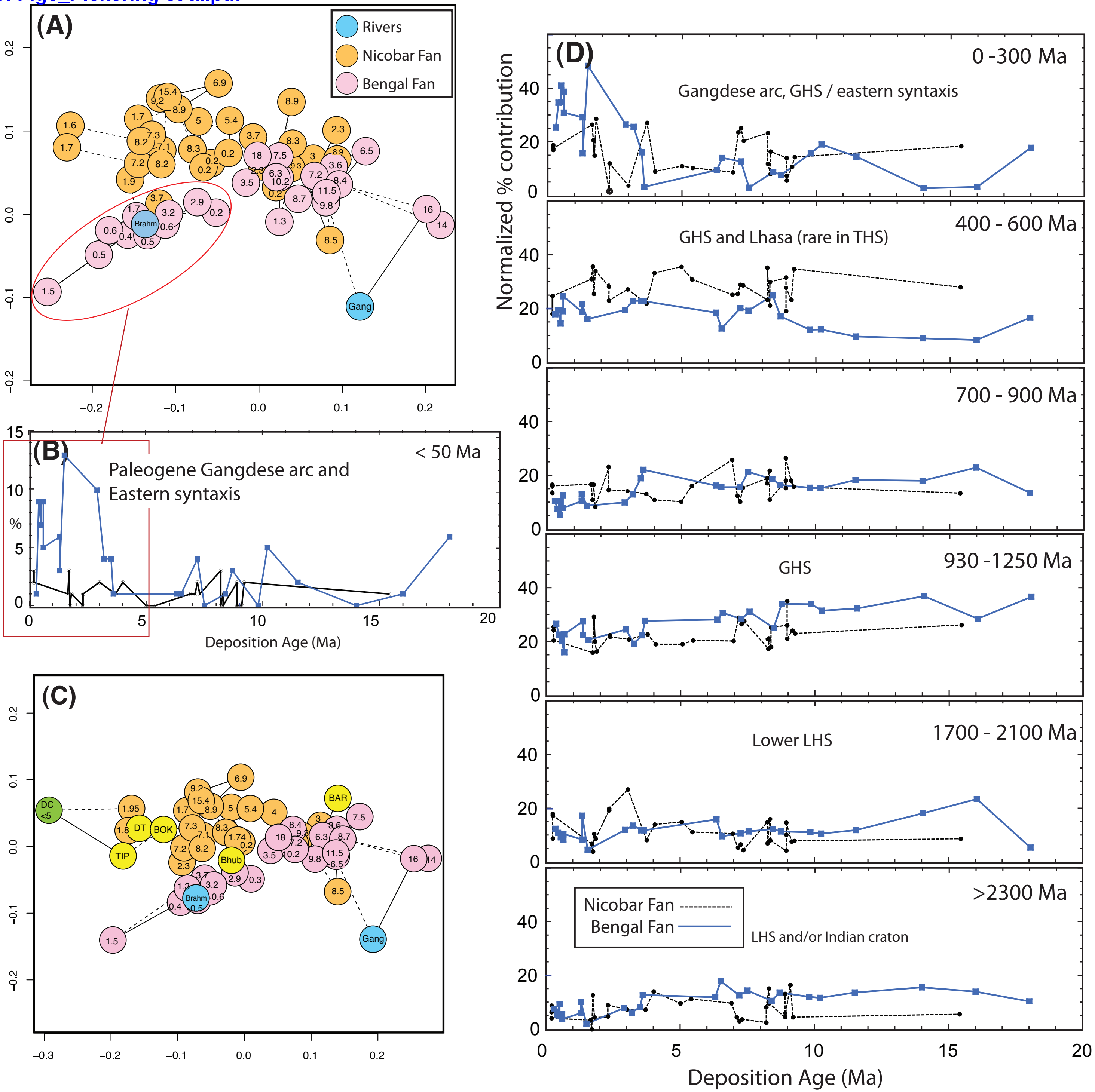

Figure 7
Click here to download Figure: Fig7_Pickering et al.pdf

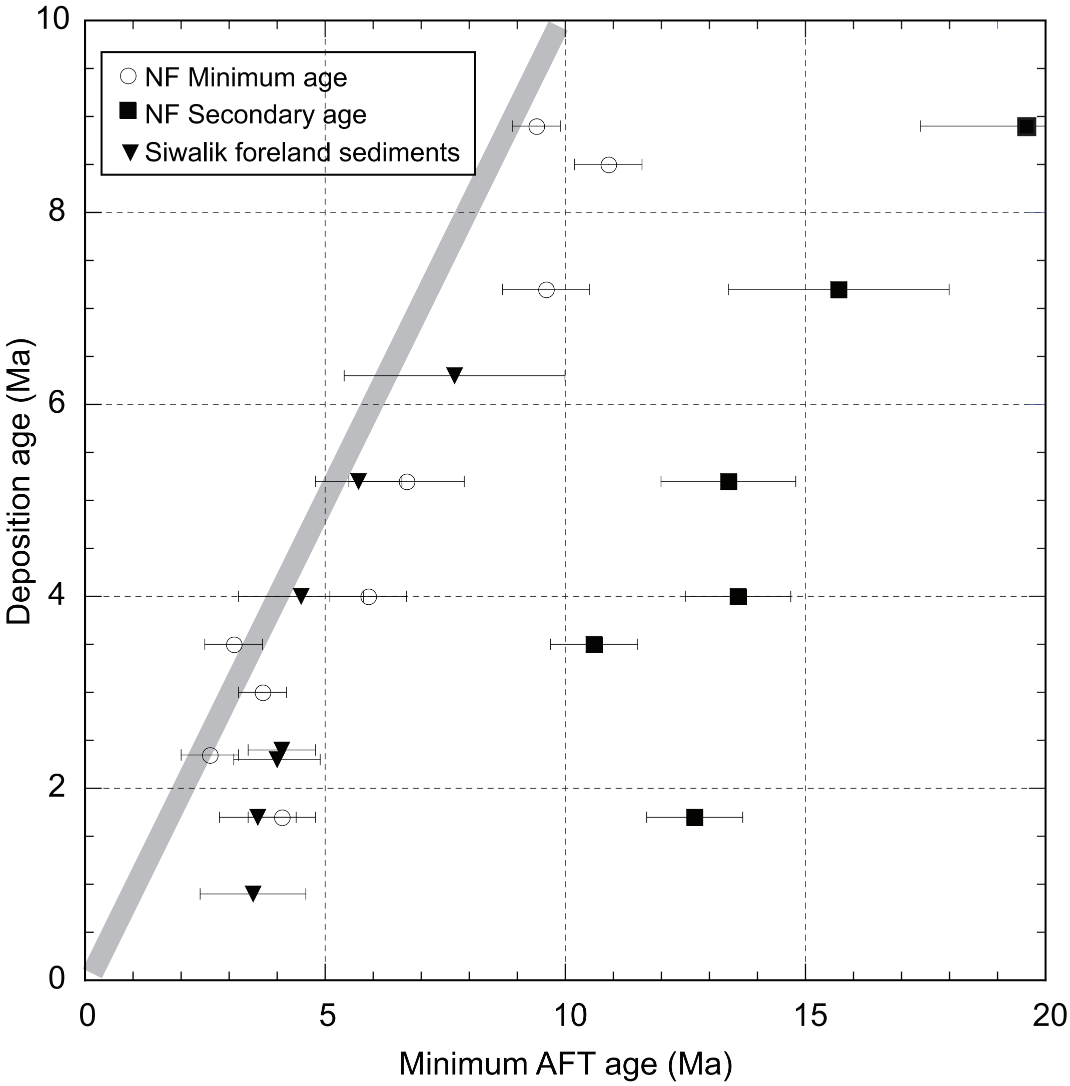

Figure 8

Click here to download Figure: Fig8_Pickering et al.pdf

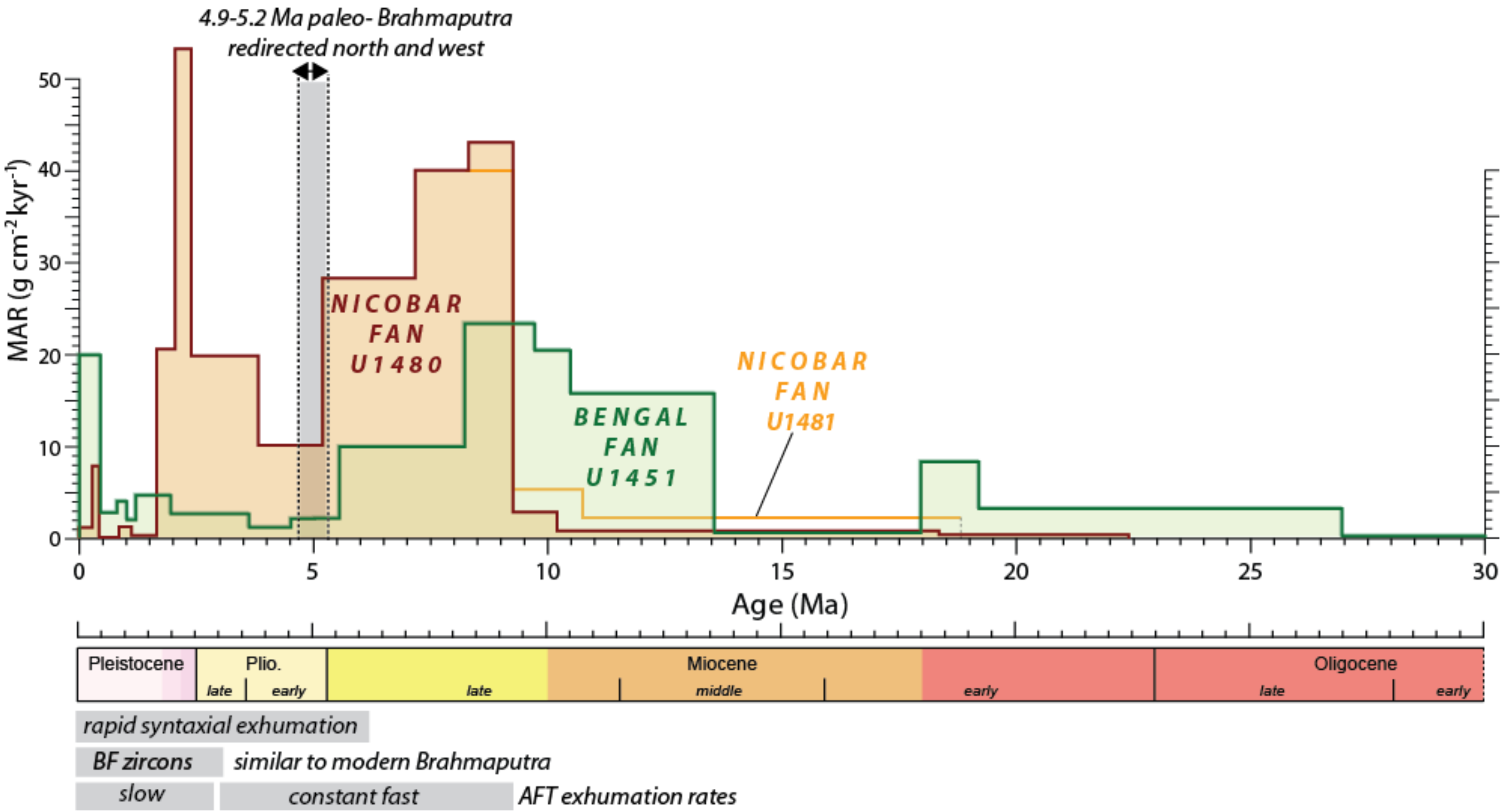

Figure 9

Click here to download Figure: Fig9_Pickering et al.pdf

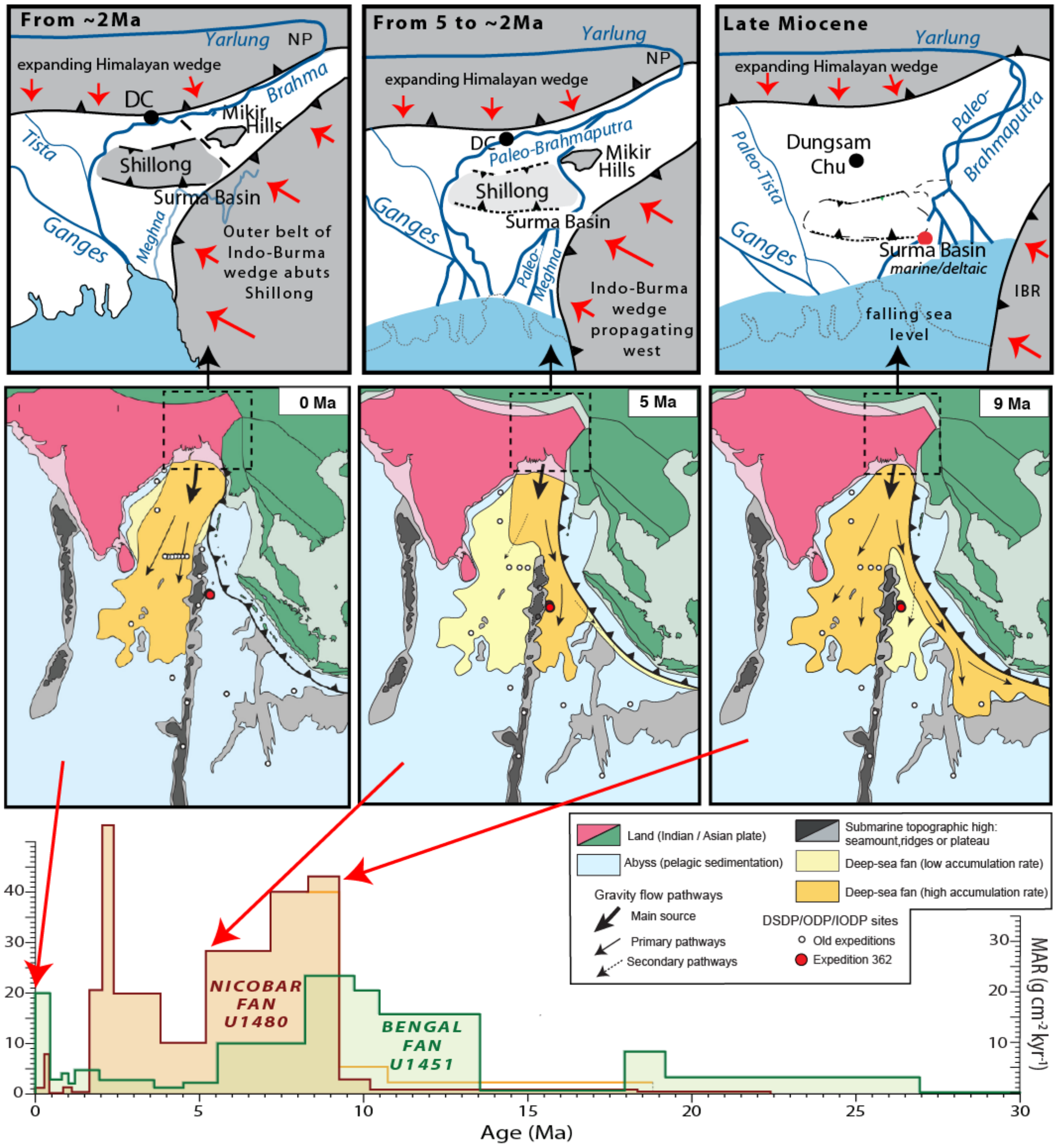

Table 1

Click here to download Table: Table 1_Pickering et al 2019.doc

Lab No	Deposit-ional Age	No. of grains	Central Age (Ma)	Age dispersion	Minimum Age (Ma)	Secondary Age (Ma)	Siwalik in Arunchal	Siwalik Eastern Bhutan
	0.9						3.5±1.1	
362-3	*1.6*	*66*	*7.1±0.9*	*56%*				
362-4	*1.7*	*30*	*4.8±0.8*	*84%*				
362-39	*1.7*	*50*	*5.2±0.7*	*68%*				
Combined	1.65	146	5.9±0.5	76%	4.1±0.7	12.7±1.1		3.6±0.8
362-8	*2.3*	*65*	*5.6±0.6*	*72%*			4.0±0.9	
362-11	*2.4*	*28*	*9.5±3.4*	*182%*				
Combined	2.35	93	7.0±1.1	138%	3.5±0.6			4.1±0.7
362-12	3.0	31	3.7±0.5	20%	3.7±0.5			
362-13	3.5	48	7.9±2.9	251%	3.1±0.6			
362-14	4.0	47	6.4±0.6	41%	5.9±0.8			4.5±1.3
362-15	*5.0*	*41*	*6.8±0.8*	*55%*				
362-16	*5.4*	*55*	*9.1±0.7*	*38%*				
Combined	5.2	96	8.2±0.6	47%	6.7±1.2	13.4±1.4		5.7±0.9
	6.3						7.7±2.3	
362-22	7.2	85	9.1±0.7	38%	9.6±0.9	15.7±2.3		
362-43	8.5	52	10.9±0.7	9%	10.9±0.7			
362-35	*8.9*	*45*	*8.9±0.6*	*8%*				
362-44	*8.9*	*21*	*9.0±1.1*	*7%*				
362-45	*8.9*	*50*	*9.5±0.9*	*44%*				
362-46	*9.0*	*61*	*11.8±1.0*	*36%*				
Combined	8.95	177	10.1±0.5	33%	9.4±0.6	19.6±2.6		